Available online at www.sciencedirect.com
SCIENCE DIRECT®
Microelectronics Reliability 46 (2006) 432–439
MICROELECTRONICS RELIABILITY
www.elsevier.com/locate/microrel

# Effects of process conditions on reliability, microstructure evolution and failure modes of SnAgCu solder joints

Periannan Arulvanan [a], Zhaowei Zhong [b,*], Xunqing Shi [a]

[a] *Singapore Institute of Manufacturing Technology, 71 Nanyang Drive, Singapore 638075, Singapore*
[b] *School of Mechanical and Aerospace Engineering, Nanyang Technological University, 50 Nanyang Avenue, Singapore 639798, Singapore*

Received 15 September 2004; received in revised form 8 April 2005
Available online 16 June 2005

**Abstract**

In this study, microstructure evolution at intermetallic interfaces in SnAgCu solder joints of an area array component was investigated at various stages of a thermal cycling test. Failure modes of solder joints were analyzed to determine the effects of process conditions on crack propagation. Lead-free printed-circuit-board (PCB) assemblies were carried out using different foot print designs on PCBs, solder paste deposition volume and reflow profiles. Lead-free SnAgCu plastic-ball-grid-array (PBGA) components were assembled onto PCBs using SnAgCu solder paste. The assembled boards were subjected to the thermal cycling test (−40 °C/+125 °C), and crack initiation and crack propagation during the test were studied. Microstructure analysis and measurements of interface intermetallic growth were conducted using samples after 0, 1000, 2000 and 3000 thermal cycles. Failures were not found before 5700 thermal cycles and the characteristic lives of all solder joints produced using different process and design parameters were more than 7200 thermal cycles, indicating robust solder joints produced with a wide process window. In addition, the intermetallic interfaces were found to have Sn–Ni–Cu. The solder joints consisted of two Ag–Sn compounds exhibiting unique structures of Sn-rich and Ag-rich compounds. A crystalline star-shaped structure of Sn–Ni–Cu–P was also observed in a solder joint. The intermetallic thicknesses were less than 3 μm. The intermetallics growth was about 10% after 3000 thermal cycles. However, these compounds did not affect the reliability of the solder joints. Furthermore, findings in this study were compared with those in previous studies, and the comparison proved the validity of this study.


## 1. Introduction

Increasing demands for miniaturization and high electrical performance have led to significant advances in integrated circuit (IC) fabrication and electronics packaging [1–3]. Processing of silicon wafers also plays a more important role in manufacturing of microelectronics and micro-electro-mechanical systems [4].

SnPb solders are widely used to make electronic interconnections for decades. Their material properties and mathematical models for reliability prediction and the behavior of SnPb solder joints are known readily.

* Corresponding author. Tel.: +65 6790 5588; fax: +65 6791 1859.
*E-mail address:* mzwzhong@ntu.edu.sg (Z. Zhong).

0026-2714/$ - see front matter © 2005 Elsevier Ltd. All rights reserved.
doi:10.1016/j.microrel.2005.05.005

The components of SnPb systems are completely soluble in the liquid state but only partially soluble in the solid state, which is common in binary systems such as copper–silver, copper–tin, copper–zinc, aluminum–copper, aluminum–magnesium, etc. [5].

The solderability of component terminations is a property defining the total suitability for industrial soldering. Good solderability results in good wetting, which means the formation of a uniform, smooth, unbroken, adherent coat of solder on the base metal, without the use of highly active fluxes and without impairing the function of the parts soldered. With poor solderability, poor wetting, non-wetting, partial wetting or dewetting is observed. Sufficient solderability of the parts used in the soldering process is a major prerequisite for the success of the process [6].

Surface mount technology (SMT) has been widely adopted in recent years. Unfortunately, SMT also brings a new era of failures. Solder joints are responsible for both electrical and mechanical connections. Solder does not have adequate ductility to ensure the repeated relative displacements due to the mismatch between expansion coefficients of the chip carrier and the circuit board. Solder behavior involves a creep–fatigue interaction, making it a poor material for mechanical connections. Finding a technique to increase the service life of future connections is not the total solution. A method must be developed for predicting the remaining service life of many joints already in use [7].

Detailed solder joint fatigue models with life prediction capability are established with detailed considerations of the effects of moisture diffusion, heat transfer, thermo-mechanical stress, hygro-mechanical stress and vapor pressure induced during reflow. These fatigue models are efficient to access the solder joint reliability of new package design, saving cost, time and manpower in performing actual thermal cycling tests [8,9].

With more consumer products moving towards environmentally friendly packaging, making solder Pb-free has become an urgent task for electronics assemblies. Elimination of Pb in solder reduces not only toxicity but also the amount of radioactive elements, which are harmful and can cause malfunction of ICs through alpha ray emission. There is a definite need to find a replacement for SnPb solder [10].

There are no sufficient material and process data for lead-free solder interconnections, and therefore research is widely carried out. One of the lead-free solder systems that are commonly used is SnAgCu.

There are three phases in the SnAgCu eutectic material, βSn and the intermetallics of $Ag_3Sn$ and $Cu_6Sn_5$. The equilibrium between $Ag_3Sn$ and $Cu_6Sn_5$ exists at 225 °C. The theoretical true eutectic point for the SnAgCu system lies at Sn3.4Ag0.7Cu [11].

Investigation of ball-grid-array (BGA) components [12] with Sn/3.8Ag/0.7Cu solder balls revealed an intermetallic interface of SnNiCu on NiAu pads of printed circuit boards (PCBs) after a thermal cycling test (−55 °C to +125 °C). The solder joint failures started occurring before 2000 cycles of the thermal cycling test.

It was reported that lead-free solder joints had fine and stable microstructures due to the formation of small-dispersed particles and thus had higher shear strengths than SnPb solders [13]. Microstructures of Sn and plate-like $Ag_3Sn$ were observed with a dendritic Sn phase for Sn–3Ag–0.5Cu alloys, including $Cu_6Sn_5$ in Sn–Ag–Cu eutectics [14]. It was found that $Ni_3Sn_4$ was uniform and thin in Sn/3.5Ag/0.5Cu while it was thick and less regular in Sn/4.0Ag/0.5Cu under dual reflow conditions using electroless Ni–P for BGA assemblies [15].

It was shown that a Ni-based UBM (under bump metallization) was more reliable than a Cu-based UBM when used with a SnAg solder [16]. In the Cr/Cu/Cu/Ni UBM system studied, the thickness of the nickel layer was found to be an important parameter. If the Ni thickness was not sufficient, ternary intermetallic formation would be promoted along the edge of the UBM. Higher temperature exposure, such as multiple reflow cycles, increased the ternary intermetallic thickness.

This paper reports experimental studies that used SnAgCu solder for assembling plastic-ball-grid-array (PBGA) components on PCBs with NiAu finish to investigate the reliability of the solder joints made under various conditions. The process variables studied include solder pad diameter, solder paste volume and reflow peak temperature.

## 2. Materials and methodology

Design of experiments (DOE) parameters, such as PCB finish and thickness, pad size and flux used in the solder paste, were chosen to reflect the elements that are widely encountered in a production environment. PBGA 352-ball packages of 35 mm × 35 mm built with Sn4.0Ag0.5Cu (SAC) solder balls were employed. The details of the package are shown in Table 1. PCBs were designed with pad sizes of 0.56 and 0.66 mm to study the effect of the variation in standoff heights on reliability of lead-free solder joints. The PCBs had daisy chain loops along the outer rows of solder balls of the PBGA components. They were fabricated with a high-$T_g$ (170 °C) FR-4 material having electroless nickel-immersion gold (NiAu) finish, and had dimensions of 150 mm × 212 mm. The PCB pads were solder-mask non-defined.

The lead-free solder paste used had Sn3.5Ag0.7Cu (SnAgCu). The solder powder used for manufacturing the paste had particle sizes of 25–45 μm, and the flux used in the paste was 'no-clean' 'ReLo' (ANSI-J-Std-flux

Table 1
Details of the package employed

| Package type | PBGA |
|---|---|
| Package size (mm) | $35 \times 35$ |
| Package thickness (mm) | 2.33 (nominal) |
| Bump number | 352 |
| Daisy chain bumps | Along outer rows |
| Ball pad pitch (mm) | 1.27 |
| Ball pad diameter (mm) | 0.635 |
| Ball alloy | Sn4.0Ag0.5Cu |
| Pad surface finish | NiAu |

classification). A single-sided assembly process was used to assemble the boards for testing. The volume of solder paste applied to the pads of the PCBs was controlled by using stencil thickness values of 0.125 and 0.2 mm, which are typically used for mixed component PCB assemblies in a manufacturing environment. Reflow profiles with peak temperatures of 235 °C (18 °C above the eutectic point of the solder) and 250 °C were chosen, with the soak (110–150 °C) time kept within 40 s and the reflow (above the eutectic point of the solder) time maintained for 90 s. The reflow was conducted in an air environment. The assembly matrix is shown in Table 2.

Before the full assembly of the boards, material characterization, reflow oven profiling and process validation were carried out to evaluate the quality of individual components. Sixteen PCBs were assembled with 12 PBGA components on each PCB, excluding additional quantities for microstructure and intermetallic growth studies. Solder paste printing was carried out using a semi-automatic printer. The packages were mounted using a pick and place machine, and the placed packages were inspected visually before they were reflowed in a reflow oven. Out of 240 packages assembled, only two had open-circuit failures.

A temperature cycling test (−40/+125 °C) was carried out with a ramp rate of 10–14 °C/min and 15 min of dwell time. The daisy chain resistance of the assemblies was monitored by a data acquisition system at the temperature extremes of each cycle. The failure criterion adopted was an increased resistance value of more than 300 Ω from the initial measurement.

## 3. Results

### 3.1. Thermal cycling test results

All of the 190 packages tested survived after 5700 cycles of the thermal cycling test. The test was continued to 8000 cycles and the failure data were collected and analyzed using Weibull plots as shown in Table 3 and Fig. 1.

The results showed that the characteristic lives of all the packages tested were more than 7200 thermal cycles. Based on analysis of variance (ANOVA) [17] carried out using the data in Table 3, it was found that the most influential factor was stencil thickness and the least influential factor was pad size. The interaction of pad size and peak temperature was severe compared to the interactions of other factors. It was predicted that the optimum conditions to yield the maximum cycles to failure would be using a pad size of 0.66 mm, a stencil thickness of 0.2 mm and a peak reflow temperature of 235 °C.

Table 2
The assembly matrix

| Pad diameter (mm) | 0.56 | | | | 0.66 | | | |
|---|---|---|---|---|---|---|---|---|
| Stencil thickness (mm) | 0.125 | | 0.2 | | 0.125 | | 0.2 | |
| Reflow peak temperature (°C) | 235 | 250 | 235 | 250 | 235 | 250 | 235 | 250 |
| Number of PCBs | 2 | 2 | 2 | 2 | 2 | 2 | 2 | 2 |
| Components assembled | 24 | 24 | 24 | 24 | 24 | 24 | 24 | 24 |

Table 3
Summary of thermal cycling test results analyzed with Weibull plots shown in Fig. 1

| Plot No. | Pad size (mm) | Stencil thickness (mm) | Peak reflow temperature (°C) | Eta (cycles) | Beta (slope) |
|---|---|---|---|---|---|
| 1 | 0.56 | 0.125 | 235 | 7576 | 10.7 |
| 2 | 0.66 | 0.125 | 235 | 7375 | 13.5 |
| 3 | 0.56 | 0.125 | 250 | 7780 | 11 |
| 4 | 0.66 | 0.125 | 250 | 8085 | 10.5 |
| 5 | 0.56 | 0.2 | 235 | 7500 | 12.1 |
| 6 | 0.66 | 0.2 | 235 | 7718 | 19.8 |
| 7 | 0.56 | 0.2 | 250 | 7356 | 21.5 |
| 8 | 0.66 | 0.2 | 250 | 7205 | 14.8 |

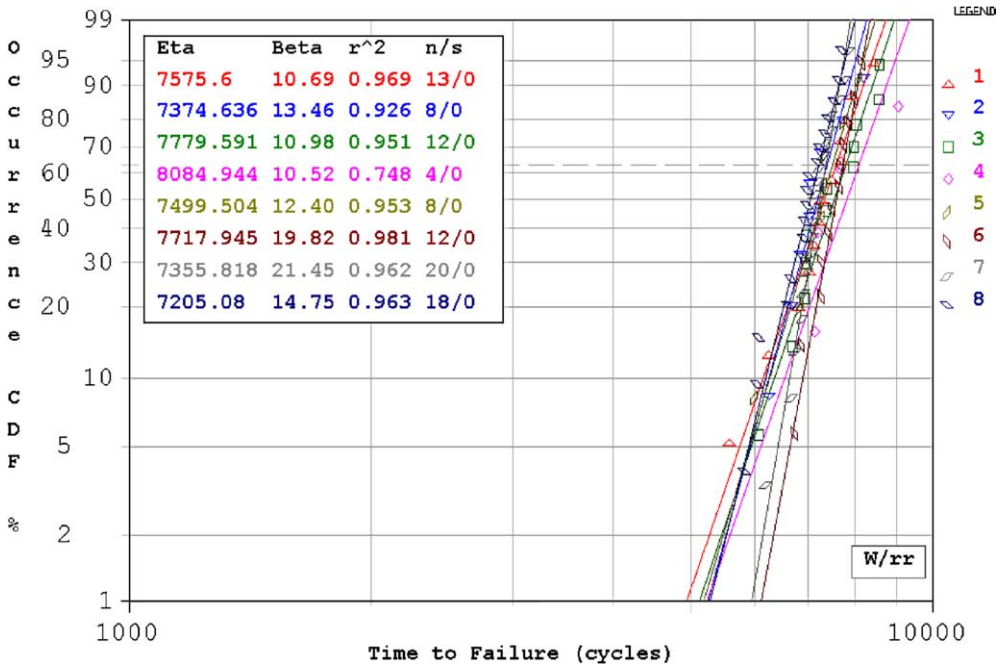


Fig. 1. Weibull plots of the thermal cycling test results.

### 3.2. Failure analysis

Thermal cycled samples were removed from the testing chamber after 500, 1000, 2000 and 3000 cycles. Micro-sections were prepared by cutting the packages diagonally, and were analyzed to determine the effects of the location of solder balls on the crack initiation and growth mechanism.

The PBGA substrate had solder-mask-defined (SMD) pads, and the PCB had non-solder-mask-defined (NSMD) pads. Robust solder joints were observed on the micro-sections of the samples before thermal cycling. The solder was reflowed along the sides of the PCB pad uniformly with a clear fillet around the pad. Reflowed solder joints were found to have good quality without any voids.

Although there was no electrical failure in the daisy chain loops before 5700 thermal cycles, potential failure modes of solder joints could be seen from the pictures of the micro-sections after certain thermal cycles. No crack initiation was observed after 500 cycles of the test, but crack initiation was obvious after 1000 thermal cycles.

Figs. 2 and 3 show crack initiation locations after 1000 cycles, and Figs. 4 and 5 show crack propagation after 3000 cycles. Cracks originated at one of the solder-joint corners at the component SMD-pad side. These corners had a high strain compared to the PCB side with NSMD pads. Solder extended along the

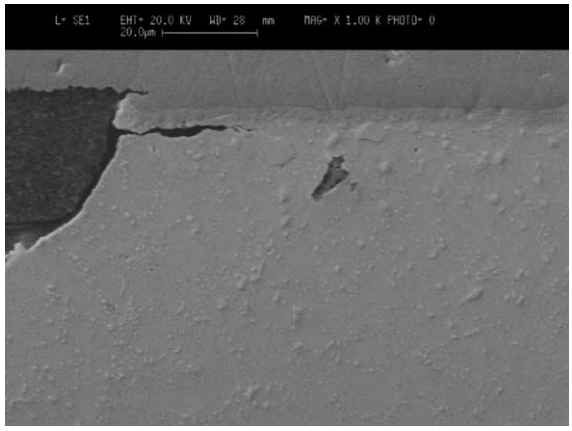

Fig. 2. Crack initiation after 1000 thermal cycles (0.2-mm stencil thickness, 235 °C reflow, 0.66-mm pad size).

periphery of the NSMD pads at the PCB side, forming a more robust structure.

The spalling of solder joints was observed at only certain locations in the samples immediately after 2000 thermal cycles, while it was predominant in the samples after 3000 cycles. Crack initiation was found in the bulk solder near the intermetallic interface, and crack propagation was found along the interface of the bulk solder and the intermetallic layer. The variations in pad size

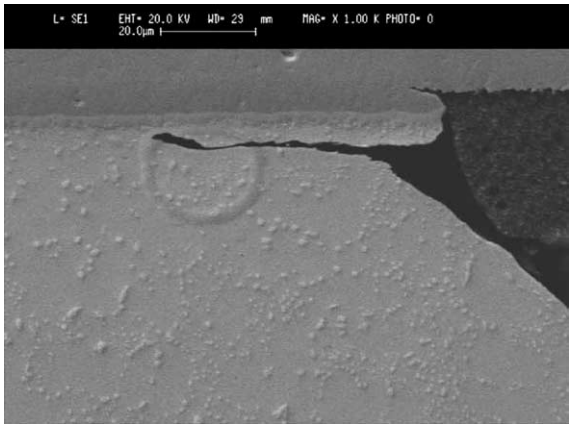


Fig. 3. Crack initiation after 1000 thermal cycles (0.125-mm stencil thickness, 250 °C reflow, 0.56-mm pad size).

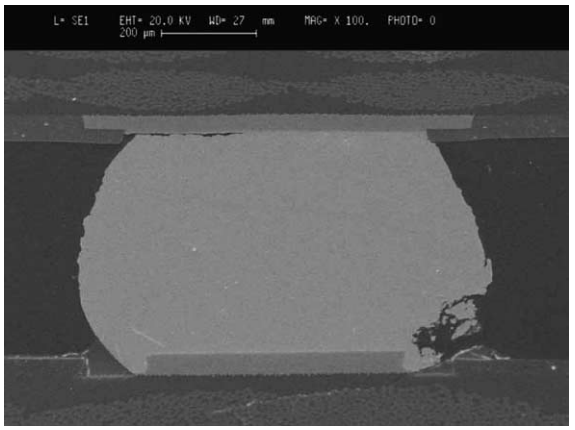


Fig. 4. Crack after 3000 thermal cycles (0.2-mm stencil thickness, 250 °C reflow, 0.56-mm pad size).

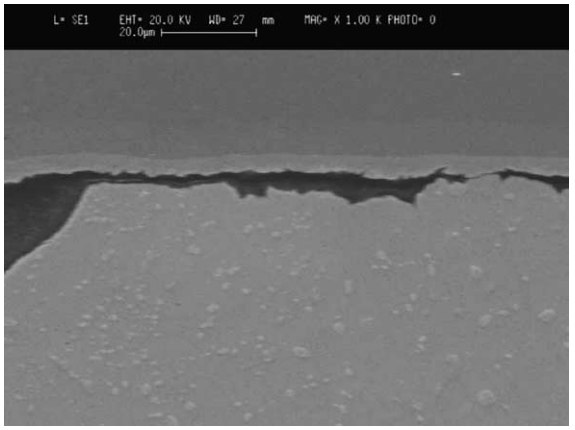


Fig. 5. SEM picture with a high magnification showing a crack after 3000 thermal cycles (0.2-mm stencil thickness, 250 °C reflow, 0.56-mm pad size).

and solder paste volume did not influence solder joint failures significantly. The influence of pad size combined with volume of solder paste printed, leading to a variation of 5% in solder joint height, did not result in distinguishable variations in failures. The reflow profiles with 235 and 250 °C peak temperatures did not cause any significant changes in failure modes either. This study confirmed that SnAgCu solder joints could be produced with a wide process window without having any significantly bad effect on the product reliability.

### 3.3. Microstructure evolution and intermetallics growth

Additional samples were prepared for microstructure analysis, and intermetallic growth characteristics were studied after various cycles of the thermal cycling test. Microstructures of solder joints were analyzed using scanning electron microscopy (SEM) and energy dispersive spectroscopy (EDS) techniques. Electroless-nickel-immersion-gold (ENIG) surface finish on both substrate and PCB pads resulted in intermetallic interface layers of Sn–Ni–Cu at both ends of a solder joint. The thicknesses of the intermetallic interface layers at the PCB and substrate sides had averages of 2.3 and 2.7 μm, respectively. The intermetallic interfaces had coarse surfaces facing the solder joint. Some sharp protrusions were observed to have broken off from the interfaces and dispersed as particles in the solder along the interfaces. The reflowed solder mainly consisted of Sn matrix with Ag–Sn intermetallics of two types.

An SEM image of a typical microstructure of the solder joints is shown in Fig. 6. The Sn-rich (type-1, Fig. 7) Sn–Ag intermetallic compound existed in abundance along grain boundaries of the Sn matrix as small worm-shaped compounds. Another Ag-rich Ag–Sn (type-2) intermetallic compound existed as a big crystalline rod-shaped structure extending across many grains at random locations. An SEM image of the type-2 Ag–Sn compound is shown in Fig. 8. The Sn–Ag type-1 compound existed uniformly across the whole solder joint along grain boundaries, while the Ag–Sn type-2 compound was not commonly found in all solder joints. A star-shaped P–Sn–Ni–Cu structure was observed in one solder joint after 3000 thermal cycles, as shown in Fig. 8.

SEM images were taken to study solder joints made under different experimental conditions, and were used to measure the intermetallic thickness with the aid of an image analyzer. For each category, measurements were conducted at three different locations and an average was derived over a range of thermal cycles (0–3000 cycles). Solder joint profiles and the microstructures were analyzed to determine if there were any significant differences due to different solder paste volume, solder pad diameters and reflow temperatures.

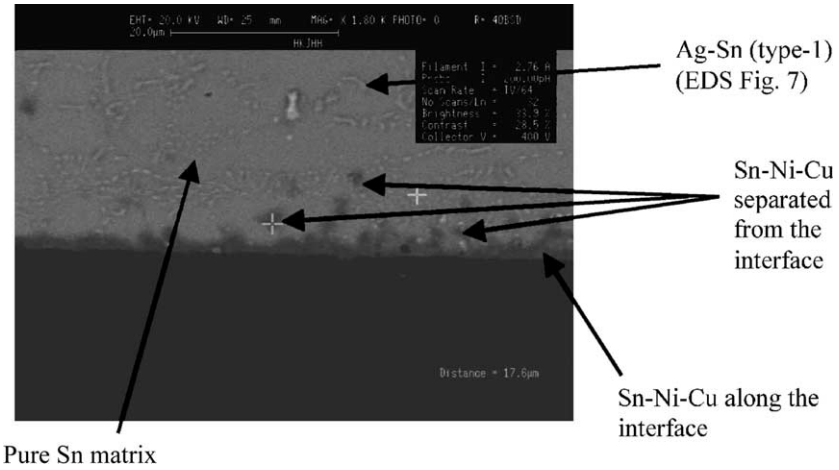


Fig. 6. Microstructure of a solder joint at the PCB-side interface.

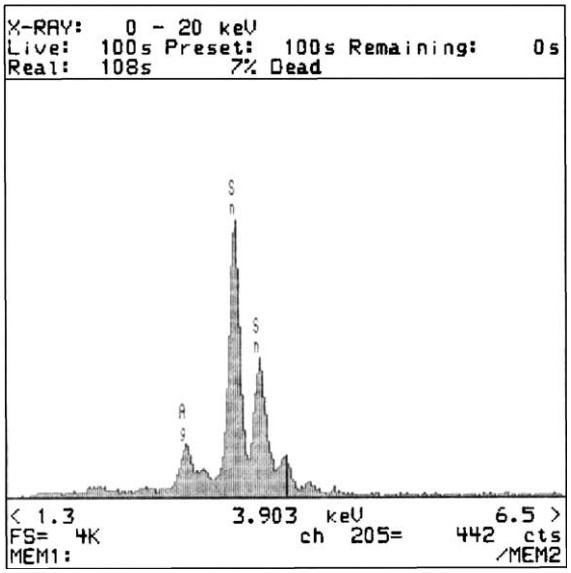


Fig. 7. EDS result of the Sn-rich (type-1) Sn–Ag intermetallic compound.

The microstructures at the interface of the PBGA substrate pad and solder joint were found to be the same as those at the interface of the PCB pad side, containing Sn–Ni–Cu intermetallics, 2–3 μm thick in all of the solder joints investigated. The intermetallics growth at both the PCB and substrate sides after 3000 thermal cycles was less than 10%. In addition, the intermetallics at the PBGA substrate side was 10% thicker than that at the PCB side. When thermal cycling continued, the Ag–Sn type-1 ''worms'' broke to form globular shapes and their sizes grew, which can be seen from the SEM images shown in Figs. 9 and 10.

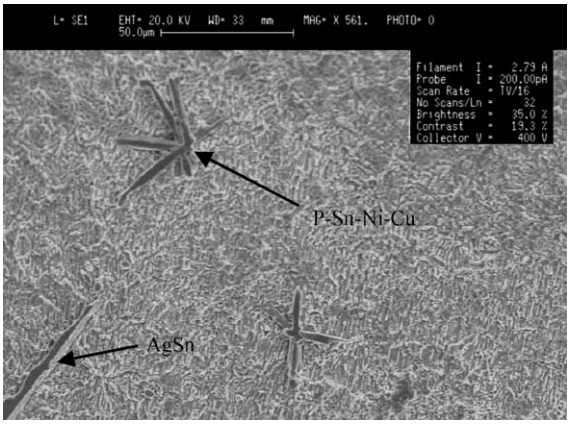


Fig. 8. Type-2 AgSn and P–Sn–Ni–Cu structures (after 3000 thermal cycles).

### 3.4. Discussion

Findings in this study were compared with those in previous studies [18–22], and Table 4 summarizes this comparison.

The results of the investigation performed by Ye et al. [18] agreed with the findings of the Ag–Sn type-1 structure in this study. They found another precipitate of $Cu_6Sn_5$ having a hexagonal crystal structure with a grain size of 0.3 μm mainly distributed in the Sn matrix, which was not found in this study. The Ag–Sn (type-2) structure found in this study was not found by Ye et al. In the study conducted by them, the solder was heated up to 280 °C before it was cooled down to the room temperature, while in our study, PCBs were reflowed at not more than 250 °C. In addition, finely dispersed voids along the intermetallic layer reported by Ye et al. were not found in our solder joints.

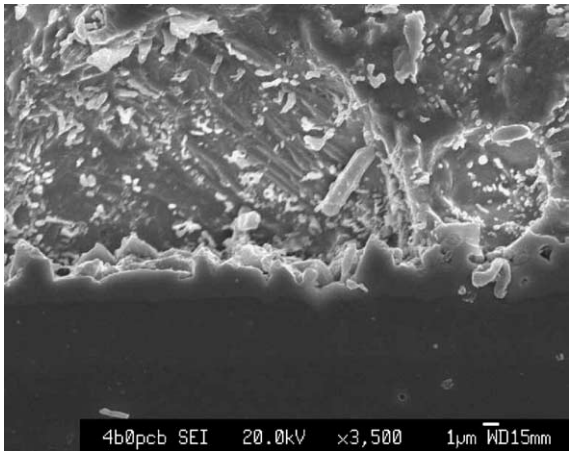


Fig. 9. SEM image of the solder joint interface at the PCB side before thermal cycling.

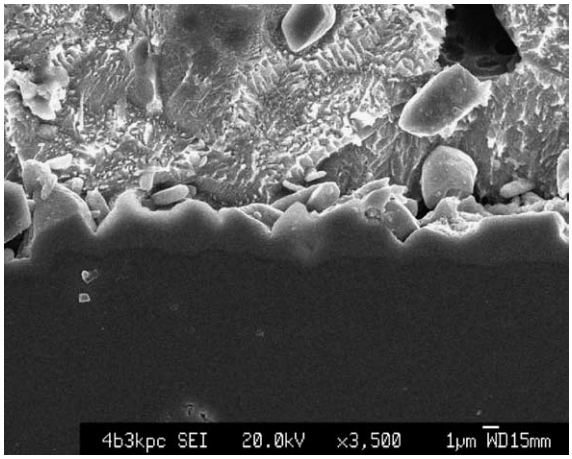


Fig. 10. SEM image of the solder joint interface at the PCB side after 3000 thermal cycles.

Microstructure evolution studies conducted by Dunford et al. [19] revealed that (Ni,Cu)/Sn intermetallic compounds at the interface of ENIG had a needle-like structure. They found that the layer consisted of $(Ni,Cu)_6Sn_5$, $(Ni,Cu)_3Sn$ and a layer of $Ni_3Sn$ that increased in thickness as thermal cycling progressed, while our study did not show any distinguishable intermetallic compounds within Sn–Ni–Cu layers at both the PCB-side and substrate-side interfaces. The type-2 Ag–Sn plates found in our study can be confirmed to be the same as the $Ag_3Sn$ plates identified by them. They also noted that early failures (180–400 cycles of −40 °C to +125 °C) occurred at the component interfaces due to the clean separation across the entire solder joint at the interface of Ni and solder of the ENIG surface finish with SAC solder. In their case, a phosphorous-rich layer was seen as a dark band at the outer surface of the Ni layer and was found on all ENIG plated surfaces, while such a phenomenon was not encountered in this study. The failure modes observed were more progressive and gradual with almost clear separation of the bulk solder from the intermetallic compound at the substrate side after 3000 thermal cycles. In-line with our findings, small secondary cracks and spalling of solder were observed by them as well. They reported Ni/Au finish produced numerous small voids around the intermetallic formation, which was not seen to occur in this study. This study showed that very few voids were present and they did not pose any significant threat to the reliability.

In a similar study carried out by Roubaud et al. [20], intermetallic compounds at the interfaces consisting of Cu–Sn were present. Another study performed by Shiau et al. [21] reported presence of the Cu–Au–Ni–Sn compound. These compounds were not present in the samples examined in this study. The failure mechanisms are in concurrence with the conclusion drawn in the paper of Stam and Davitt [22]. Although microstructure differences could be seen between the lead-free and lead

Table 4
Comparison of findings in this study and previous studies [18–22]

| Phenomena | This study | Previous study | Ref. |
|---|---|---|---|
| Ag–Sn type-1 structure | Found | Found | [18] |
| $Cu_6Sn_5$ having a hexagonal crystal structure | Not found | Found | [18] |
| Ag–Sn (type-2) structure | Found | Not found | [18] |
| Finely dispersed voids | Not found | Found | [18] |
| Intermetallic compounds within Sn–Ni–Cu layers | Not found | Found | [19] |
| Ag–Sn (type-2) structure | Found | Found | [19] |
| A phosphorous-rich layer as a dark band | Not found | Found | [19] |
| Small secondary cracks and spalling of solder | Found | Found | [19] |
| Ni/Au finish produced small voids around intermetallic formations | Not found | Found | [19] |
| Intermetallic compounds at the interfaces consisting of Cu–Sn | Not found | Found | [20] |
| Cu–Au–Ni–Sn compound | Not found | Found | [21] |
| Failure mechanisms | Agreed | Agreed | [22] |

bearing solder joints, similar solder-joint failure mechanisms occurred.

## 4. Conclusions

Lead-free PCB assemblies were carried out using different foot print designs on PCBs, solder paste deposition volume and solder reflow profiles. Lead-free PBGA assemblies were accomplished with nearly 100% assembly yield. Assembled boards were subjected to a thermal cycle test of −40 to +125 °C and no failures were found before 5700 thermal cycles. The characteristic lives of all solder joints produced using different process and design parameters were more than 7200 thermal cycles, indicating robust solder joints produced with a wide process window. ANOVA revealed that the most influential factor was stencil thickness. The optimal conditions to yield the maximum thermal cycles to failure would be a pad size of 0.66 mm, a stencil thickness of 0.2 mm and a peak reflow temperature of 235 °C.

Crack initiation and propagation occurred along the interface between the bulk solder and the intermetallic layer in the bulk solder side. The intermetallic interfaces had a compound of Sn–Ni–Cu. Some of this compound dispersed in the bulk solder at sporadic locations. The solder joints consisted of two Ag–Sn compounds exhibiting unique structures of Sn-rich (type-1) and Ag-rich (type-2) compounds. As the thermal cycling continued, the Ag–Sn type-1 ''worms'' broke to form globular shapes and grew in size. A crystalline star-shaped structure of Sn–Ni–Cu–P was also observed in a solder joint. The intermetallic thicknesses were less than 3 μm. The intermetallics growth was about 10% after 3000 thermal cycles. The compounds did not affect the reliability of solder joints. Findings in this study were compared with those in previous studies, and the comparison proved the validity of this study.

## References

[1] Zhong Z. Stud bump bond packaging with reduced process steps. Soldering Surface Mount Technol 2001;13(2):35–8.
[2] Zhong Z. Reliability of FCOB with and without encapsulation. Soldering Surface Mount Technol 2001;13(2):21–5.
[3] Zhong Z, Yip PK. Finite element analysis of a three dimensional package. Soldering Surface Mount Technol 2003;15(1):21–5.
[4] Zhong ZW, Tok WH. Grinding of single-crystal silicon along crystallographic directions. Mater Manufact Process 2003;18(5):811–24.
[5] Manko HH. Solders and soldering, materials, design, production, and analysis for reliable bonding. New York: McGraw-Hill; 2001.
[6] Wassink RJK. Soldering in electronics: a comprehensive treatise on soldering technology for surface mounting and through-hole techniques. Scotland: Electrochemical publications; 1989.
[7] Lau JH. Solder joint reliability, theory and applications. New York: Van Nostrand Reinhold; 1991.
[8] Tee TY, Zhong Z. Integrated vapor pressure, hygroswelling, and thermo-mechanical stress modeling of QFN package during reflow with interfacial fracture mechanics analysis. Microelectron Reliab 2004;44(1):105–14.
[9] Tee TY, Zhong Z. Board level solder joint reliability analysis and optimization of pyramidal stacked die BGA packages. Microelectron Reliab 2004;44(12):1957–65.
[10] Zhong ZW, Chan KC, Chen YH. Characterization of electroplated eutectic Sn–Ag solder bumps. Int J Comput Eng Sci 2003;4(3):733–6.
[11] National Institute of Standards and Technology (NIST) database. Phase diagrams and computational thermodynamics. Available from: http://www.metallurgy.nist.gov/phase/solder/agcusn.html, accessed on 12 September 2004.
[12] Anand A, Mui YC. Lead-free solder evaluations for ball attaché process. In: Proceedings of 4th electronic packaging technology conference, Singapore, 2002. p. 6–10.
[13] Ye LL, Lai Z, Liu J, Tholen A. Microstructural coarsening of lead-free solder joints during thermal cycling. In: Proceedings of electronic components and technology conference, Las Vegas, USA, 2000. p. 134–7.
[14] Mutoh Y, Zhao J, Miyashita Y, Kanchanomai C. Fatigue crack growth behavior of lead-containing and lead-free solders. Soldering Surface Mount Technol 2002;14(3):37–45.
[15] Minogue GR. A thermodynamic and kinetic comparison of Sn–Pb and non-Pb solders for BGA applications. In: Proceedings of technical conference APEX 2002, San Diego, CA, 2002. p. S06 3.1–3.6.
[16] Chan KC, Zhong ZW, Ong KW. Study of under bump metallization barrier layer for lead-free solder. Soldering Surface Mount Technol 2003;15(2):46–52.
[17] Ross PJ. Taguchi techniques for quality engineering. New York: McGraw-Hill Book Company; 1988.
[18] Ye L, Lai ZH, Liu J, Tholen A. Microstructure investigation of Sn–0.5Cu–3.5Ag and Sn–3.5Ag–0.5Cu–0.5B lead-free solders. Soldering Surface Mount Technol 2001;13(3):16–20.
[19] Dunford SO, Primavera A, Meilunas M. Microstructural evolution and damage mechanisms in Pb-free solder joints during extended −40 °C to 125 °C thermal cycles. Technical article, IPC review magazines, December 2002, 8–9 and January 2003. p. 10–1.
[20] Roubaud P, Ng G, Henshall G, Bulwith R. Herber R, Prasad S, et al. Impact of intermetallic growth on the mechanical strength of Pb-free BGA assemblies. In: Proceedings of technical conference APEX 2001, San Diego, CA, 2002. p. LF2–3.
[21] Shiau LC, Ho CE, Kao CR. Reactions between Sn–Ag–Cu lead-free solders and the Ni–Au surface finish in advanced electronic packages. Soldering Surface Mount Technol 2002;14(3):25–9.
[22] Stam FA, Davitt E. Effects of thermomechanical cycling on lead and lead-free (SnPb and SnAgCu) surface mount solder joints. Microelectron Reliab 2001;41:1815–22.